AIChE

A CFD Study of Gas–Solid Jet in a CFB Riser Flow

Tingwen Li
National Energy Technology Laboratory, U.S. Department of Energy, WV 26507

URS Corporation, Morgantown, WV 26505

Chris Guenther
National Energy Technology Laboratory, U.S. Department of Energy, WV 26507

DOI 10.1002/aic.12619
Published online May 16, 2011 in Wiley Online Library (wileyonlinelibrary.com).

Three-dimensional high-resolution numerical simulations of a gas–solid jet in a high-density riser flow were conducted. The impact of gas–solid injection on the riser flow hydrodynamics was investigated with respect to voidage, tracer mass fractions, and solids velocity distribution. The behaviors of a gas–solid jet in the riser crossflow were studied through the unsteady numerical simulations. Substantial separation of the jetting gas and solids in the riser crossflow was observed. Mixing of the injected gas and solids with the riser flow was investigated and backmixing of gas and solids was evaluated. In the current numerical study, both the overall hydrodynamics of riser flow and the characteristics of gas–solid jet were reasonably predicted compared with the experimental measurements made at NETL. Published 2011 American Institute of Chemical Engineers *AIChE J,* 58: 756–769, 2012

Keywords: computational fluid dynamics, circulating fluidized bed, gas–solid jet, flow hydrodynamics, mixing

Introduction

Circulating fluidized beds (CFBs) have been widely used in chemical, petrochemical, metallurgical, environmental, and energy industries including fossil fuel combustion, coal and biomass gasification, and fluid catalytic cracking (FCC). The CFB process possesses a number of unique features that make it more attractive than other systems in the energy industries. For example, CFB technology offers significant advantages such as fuel flexibility, increased through-put, in-bed sulfur capture, and relatively low NO_X emissions with high efficiencies in combustion and gasification. Among these applications, gasification is a promising technology for coal, biomass, and waste utilization with low environmental impact, reducing global CO_2 emissions, which will be the centerpiece of tomorrow's advanced power plants. This technology is also being considered for sorbent based CO_2 capture.

In gasification process, the coal particles are usually injected into the gasifier with high-speed gas flow as gas–solid jets. It is of great practical importance to understand the manner in which the coal particles disperse and mix with the bed materials on entering the system. Although there has been considerable study of the gas jet penetration and mixing in fluidized beds,[1–5] only limited work on a two-phase jet flow in fluidized beds can be found in the literature, which is mostly on the gas–liquid injection into different gas–solid systems.[6–9] There are fewer studies of particle-laden jets in fluidized beds. Glicksman et al.[10] studied the mixing characteristics of horizontally injected particles in a one-quarter scale model of a pressurized bubbling fluidized bed combustor using a thermal tracer technique. It was reported that the lateral motion of the injected particles was much greater than the lateral motion of an injected gas jet. Shadle et al.[11] studied

Correspondence concerning this article should be addressed to T. Li at tingwen.li@ur.netl.doe.gov.

the jet penetration of a gas–solid jet into a circulating fluidized bed riser by tracking the phosphorescent particles illuminated immediately prior to injection. The extent of radial penetration of the solid particles was measured at different downstream levels and effects of several operating conditions including jet velocity, jet solids concentration, riser flow regime were investigated. Wang et al.[12] reported dynamic phenomena of the three-dimensional (3-D) horizontal gas and gas/solids mixture jets in a bubbling fluidized bed with an electrical capacitance volume tomography (ECVT) technique. The shape of gas–solid jet and penetration depth were investigated which were shown to be different from the gas jet. However, even with the most advanced experimental techniques, it is too difficult to fully understand the flow behavior of particle-laden jets in a gas–solid flow system.

With the significant improvements in computational power and numerical algorithms, computational fluid dynamics (CFD) has become a valuable tool for studying the complex phenomena in single-phase and multiphase flows. Remarkable progress has been made recently in CFD modeling of gas–solid fluidized beds. CFD modeling not only saves time and money for construction and operation of complex pilot-scale reactors but also provides the detailed information needed to optimize industrial designs and troubleshoot operational problems, which are usually difficult even impossible to be measured in experiments with available techniques.[13] On the other hand, CFD can be used as an important tool together with experiments to improve our understanding of many fundamental problems in multiphase flows.[14] Gas–solid injection has been encountered in the numerical modeling of gasification process. However, most of studies focused on the overall gasification performance and no much attention was paid to the gas–solid jetting flow in the gasifier.[15–19] In some work, trajectories of fuel particles injected into entrained flow gasifiers were reported based on Eulerian-Lagrangian simulation in which a very dilute gas–solid flow was simulated.[20,21] To better model CFB gasifiers, the gas–solid jet in a high-density riser flow needs to be simulated. Li et al.[22] conducted numerical simulations of coal injection into a reduced configuration of CFB gasifier. The effects of grid resolution and discretization scheme on the predictions of the general jet behavior, flow hydrodynamics, and gasification performance were analyzed. However, the complex interactions between the gas–solid jet and the riser flow were not completely captured due to the assumptions introduced in the reduced configuration of gasifier.

In this study, a gas–solid jet in a CFB riser flow is investigated through high-resolution 3-D CFD simulations of a pilot-scale experimental setup. The general hydrodynamics of the riser flow predicted by the numerical simulations are first validated against the available experimental data. Then, the fundamental characteristics of the gas–solid jet are studied through numerical results and compared against the measurements and observation from experiments. Finally, mixing of the jetting flow with the riser crossflow is evaluated.

Experiment Setup

The experiments were conducted in a 0.305-m diameter 15.9-m tall pilot-scale cold circulating fluidized system. A schematic diagram of the cold model is given in Figure 1. The high-density polyethylene (HDPE) beads with an averaged diameter of 750 μm and a density of 863 kg/m^3 were used in the experiments. This type of particles was chosen to facilitate the numerical simulations as the grid size needed by CFD simulations is commonly proportional to the particle size. The solids enter the riser from a side port 0.23 m in diameter and 0.27 m above the gas distributor. Solids exit the riser through a 0.20 m side port about 1.2 m below the top of the riser. The distance from the centerline of the solids inlet to the outlet is 15.45 m. A detailed description of the experimental facility and the process instrumentation was provided by Mei et al.[23] To study the jet penetration, a gas–solid jet was introduced through a small tube of 1.59-cm diameter at 4.3 m above the bottom distributor in the same azimuthal direction as the bulk solids feed to the riser. Same solid particles as the bulk bed material were fed through the injector with high-velocity gas flow. The overall solids circulation rate within the CFB and solids feed rate through the tube were monitored. The solids velocity at the jet inlet was measured by means of ''time of flight'' experiments. Details on the experiments can be found in the literature.[11]

Two methods were employed in the experiments to determine the penetration and distribution of injected particles: photo sensors and piezoelectric pressure transducers. Solids particles were exposed to UV light before injection into the riser. Phosphorescent glow from the jet solids was then detected by photo sensors at different radial positions within the riser 0.15 and 0.30 m above the injection. It was assumed that the voltage signal from the photo sensor is proportional to the local concentration of the tracer particles. Relative concentration distribution of the jetting particles could be obtained through the optical signals. A normalized concentration profile of the phosphorescent particles along the jet direction was then obtained through data fitting at each level. The distance from the jet wall to the maximum peak and the width of the profile at half of the peak value were reported to characterize the jet-behavior as schematically illustrated in Figure 2. Piezoelectric transducer measurements were made at the feed level along the jet direction to estimate the radial solids flux from the horizontal gas–solid jet. Decay of the measured solids flux along the jet direction was calculated to characterize the jet penetration at that level. In addition, local particle velocities were measured at various radial positions, riser heights, and azimuthal angles using an optical fiber probe. Incremental differential pressures were also measured along the riser. Four variables were tested including the jet velocity, solids feed rate into the jet, the riser velocity, and the overall CFB circulation rate over eight distinct cases as reported in the literature.[11] For each case, several runs were undertaken to make sure the reproducibility of experimental results.

Numerical Modeling

Governing equations

In this study, the Multiphase Flow with Interphase eXchanges (MFIX) code, available from the U.S. Department of Energy (DOE) National Energy Technology Laboratory (NETL) at https://mfix.netl.doe.gov, was used to conduct the numerical simulations. MFIX is a multifluid,

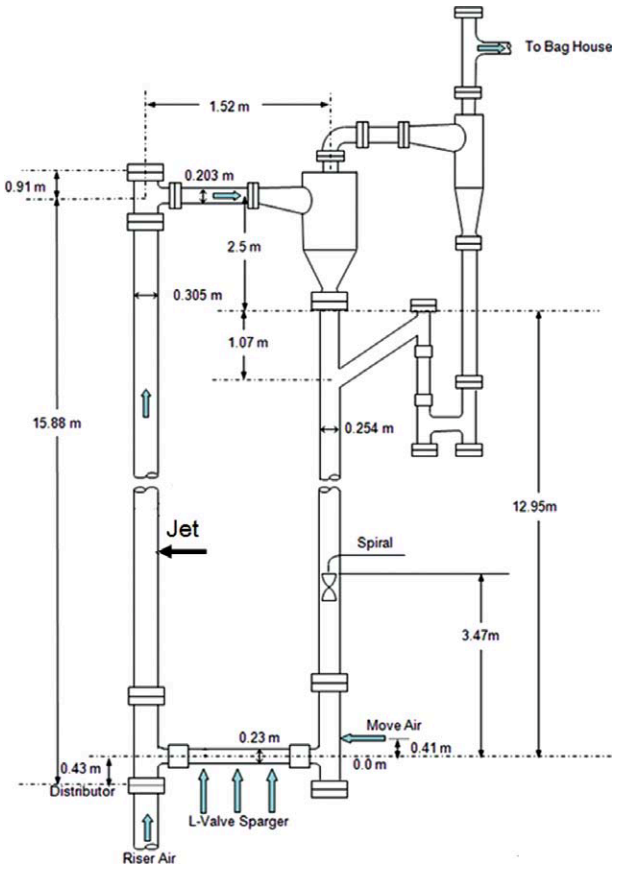

Figure 1. Schematic of NETL CFB with gas–solid jet injection.

[Color figure can be viewed in the online issue, which is available at wileyonlinelibrary.com.]

Eulerian-Eulerian code, with each phase treated as an interpenetrating continuum. Mass and momentum conservation equations are solved for the gas and solid (particulate) phases, with appropriate closure relations.[24,25] The governing equations for the solid phase are closed by kinetic granular theory, which assumes that the random motion of particles is analogous to the motion of molecules in a gas. A granular temperature, proportional to the mean square of the random particle velocity based on the Maxwellian velocity distribution, is then defined to model the fluctuating energy of the solid phase. Constitutive relations for the solid-phase stress tensor are derived based on the kinetic theory.[26–28] For flows without chemical reaction, as considered in this study, a brief summary on the hydrodynamic model equations is given in Table 1. More details were provided in the online documentations.[24]

In the above equations, the turbulence of gas phase is modeled in Eq. 10 with a simple subgrid scale model (SGS).[29] The turbulence of the gas phase is usually not of primary concern for systems with dense solids flow as the particle–particle collisions dominate the flow[30] and the inertia of particles further damps out the turbulence in the gas phase.[31,32] An algebraic Eq. 20 was used for the granular temperature to save the computational time. To study the jet behavior, additional species equations are solved to track the gas and particles injected through the jet inlet. The self-diffusion coefficient of particles in Eq. 30 proposed by Hsiau and Hunt[33] is used to model the diffusion of tracer particles in the solids crossflow. For simplicity, the effect of gas turbulence on the particle dispersion is neglected, which should be considered in the future study.

Simulation setup

A 3-D simulation of the whole riser was performed. A cuboid computational domain was discretized with a uniform grid size of 7.5 mm except at the jet injection level where the grid was slightly refined. The grid is believed to be fine enough according to the well known 10-particle-diameter criterion for grid independence in the gas–solid flow simulations.[34,35] To represent the cylindrical geometry of riser, some cells were blocked so that a stair-step surface was used to represent the column boundary. A total of 3 million computational cells were used. To better resolve the transient flow behavior of riser flows and jet injection, a second-order Superbee discretization scheme was used for solving all equations.[22,36] The computation was conducted on a high-performance computing (HPC) system with 192 Xeon quad-core CPU running at 2.83 GHz.

The material properties and operating conditions used in the numerical simulations are summarized in Table 2. In this study, only two cases were simulated with low- and high-jet gas velocities of 16 and 37 m/s, respectively. Detailed flow information at the jet inlet is given in Table 3. The other conditions are fixed for all cases.

At the bottom distributor, a uniform gas inflow was specified, with no particles entering the domain. Acknowledging the variation of superficial gas velocity along the column height, a superficial gas velocity of 7.62 m/s defined based on the bottom condition was used. While for the side solids inlet above the distributor and the gas–solid jet inlet, constant inflow conditions were imposed according to the experimental mass flow rates. At the top abrupt exit, a constant pressure was assumed and particles were free to leave the system. At the side wall, a no-slip boundary condition was adopted for both the gas and the solids phase.

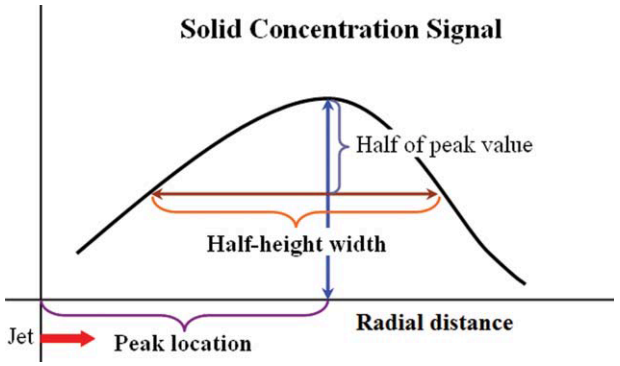

Figure 2. Schematic of experimental measurements on jet characteristics.

[Color figure can be viewed in the online issue, which is available at wileyonlinelibrary.com.]

Table 1. Summary of MFIX Equations

A. Governing equations

(a) Continuity equations

$$\frac{\partial}{\partial t}(\varepsilon_g \rho_g) + \nabla \cdot (\varepsilon_g \rho_g \vec{V}_g) = 0 \tag{1}$$

$$\frac{\partial}{\partial t}(\varepsilon_p \rho_p) + \nabla \cdot (\varepsilon_p \rho_p \vec{V}_p) = 0 \tag{2}$$

(b) Momentum equations

$$\frac{\partial}{\partial t}(\varepsilon_g \rho_g \vec{V}_g) + \nabla \cdot (\varepsilon_g \rho_g \vec{V}_g \vec{V}_g) = \nabla \cdot \bar{\bar{\tau}}_g - \varepsilon_g \nabla P + \varepsilon_g \rho_g g - I_{gp} \tag{3}$$

$$\frac{\partial}{\partial t}(\varepsilon_p \rho_p \vec{V}_p) + \nabla \cdot (\varepsilon_p \rho_p \vec{V}_p \vec{V}_p) = \nabla \cdot \bar{\bar{\tau}}_p - \varepsilon_p \nabla P + \varepsilon_p \rho_p g + I_{gp} \tag{4}$$

(c) Species equations

$$\frac{\partial}{\partial t}(\varepsilon_g \rho_g X_{gn}) + \nabla \cdot (\varepsilon_g \rho_g \vec{V}_g X_{gn}) = \nabla \cdot (D_{gn} \nabla X_{gn}) \tag{5}$$

$$\frac{\partial}{\partial t}(\varepsilon_p \rho_p X_{pn}) + \nabla \cdot (\varepsilon_p \rho_p \vec{V}_p X_{pn}) = \nabla \cdot (D_{pn} \nabla X_{pn}) \tag{6}$$

B. Constitutive equations

(a) Gas stress tensor

$$\bar{\bar{\tau}}_g = 2\mu_{ge}\bar{\bar{S}}_g \tag{7}$$

$$\bar{\bar{S}}_g = \frac{1}{2}\left(\nabla \vec{V}_g + (\nabla \vec{V}_g)^T\right) - \frac{1}{3}\nabla \cdot \vec{V}_g \bar{\bar{I}} \tag{8}$$

$$\mu_{ge} = Min\left(\mu_{max}, \mu_g + \mu_t\right) \tag{9}$$

$$\mu_t = 2l^2 \varepsilon_g \rho_g \sqrt{I_{2Dg}} \tag{10}$$

$$\bar{\bar{D}}_g = \frac{1}{2}\left(\nabla \vec{V}_g + (\nabla \vec{V}_g)^T\right) \tag{11}$$

(b) Solid stress tensor

$$\bar{\bar{\tau}}_p = \left(-P_s + \eta \mu_b \nabla \cdot \vec{V}_p\right)\bar{\bar{I}} + 2\mu_p \bar{\bar{S}}_p \tag{12}$$

$$\bar{\bar{S}}_p = \frac{1}{2}\left(\nabla \vec{V}_p + (\nabla \vec{V}_p)^T\right) - \frac{1}{3}\nabla \cdot \vec{V}_p \bar{\bar{I}} \tag{13}$$

$$P_s = \varepsilon_p \rho_p \Theta_p [1 + 4 g_0 \varepsilon_p \eta] \tag{14}$$

$$\mu_p = \left(\frac{2+\alpha}{3}\right)\left[\frac{\mu_p^*}{g_0 \eta (2-\eta)}\left(1 + \frac{8}{5}\eta g_0 \varepsilon_p\right)\left(1 + \frac{8}{5}\eta(3\eta - 2) g_0 \varepsilon_p\right) + \frac{3}{5}\eta \mu_b\right] \tag{15}$$

$$\mu_p^* = \frac{\varepsilon_p \rho_p \Theta_p g_0 \mu}{\varepsilon_p \rho_p \Theta_p g_0 + \frac{2\beta\mu}{\varepsilon_p \rho_p}} \tag{16}$$

$$\mu = \frac{5}{96}\rho_p d_p \sqrt{\pi \Theta_p} \tag{17}$$

$$\mu_b = \frac{256}{5\pi}\mu \varepsilon_p^2 g_0 \tag{18}$$

$$\eta = \frac{1+e}{2} \tag{19}$$

(c) Granular temperature

$$\Theta_p = \left[\frac{\frac{-(K_1 \varepsilon_p + \rho_p) Tr(\bar{\bar{D}}_p)}{2K_4 \varepsilon_p} + \sqrt{\frac{(K_1 \varepsilon_p)^2 Tr^2(\bar{\bar{D}}_p) + 4K_4 \varepsilon_p [2K_3 Tr(\bar{\bar{D}}_p^2) + K_2 Tr^2(\bar{\bar{D}}_p)]}{2K_4 \varepsilon_p}}}{2K_4 \varepsilon_p}\right]^2 \tag{20}$$

(*Continued*)

$$K_1 = 2(1-e)\rho_p g_0 \tag{21}$$

$$K_2 = \frac{4}{3\sqrt{\pi}} d_p \rho_p (1+e) g_0 \varepsilon_p - \frac{2}{3}K_3 \tag{22}$$

$$K_3 = \frac{d_p \rho_p}{2}\left\{\frac{\sqrt{\pi}}{3(3-e)}\left[\frac{(3e+1)}{2} + \frac{2}{5}(1+e)(3e-1) g_0 \varepsilon_p\right] + \frac{8\varepsilon_p}{5\sqrt{\pi}} g_0 (1+e)\right\} \tag{23}$$

$$K_4 = \frac{12(1-e^2)\rho_p g_0}{d_p \sqrt{\pi}} \tag{24}$$

(d) Inter-phase momentum exchange

$$I_{gp} = \beta\left(\vec{V}_g - \vec{V}_p\right) \tag{25}$$

$$\beta = \begin{cases} 150\frac{\varepsilon_p^2 \mu_g}{\varepsilon_g d_p^2} + 1.75\frac{\varepsilon_p \rho_g \left|\vec{V}_p - \vec{V}_g\right|}{d_p} & \text{if } \varepsilon_p > 0.2 \\ \frac{3}{4} C_d \varepsilon_g^{-2.65} \frac{\varepsilon_p \varepsilon_g \rho_g \left|\vec{V}_p - \vec{V}_g\right|}{d_p} & \text{if } \varepsilon_p \le 0.2 \end{cases} \tag{26}$$

$$C_d = \begin{cases} \frac{24}{Re \cdot \varepsilon_g}\left(1 + 0.15(Re \cdot \varepsilon_g)^{0.687}\right) & \text{if } Re \cdot \varepsilon_g < 1000 \\ 0.44 & \text{if } Re \cdot \varepsilon_g \ge 1000 \end{cases} \tag{27}$$

$$Re = \frac{\rho_g \left|\vec{V}_p - \vec{V}_g\right| d_p}{\mu_g} \tag{28}$$

(e) Gas and solid diffusivity

$$D_g = \rho_g D_{g0} + \frac{\mu_t}{Sc_t} \tag{29}$$

$$D_p = \frac{\rho_p d_p \sqrt{\pi \Theta_p}}{8(1+e_p)\varepsilon_p g_0} \tag{30}$$

$$Sc_t = 0.7 \tag{31}$$

Initially, the whole riser was uniformly filled with solid particles at a volume fraction of 0.1. Gas and solids flows were introduced through the bottom distributor and the solids feed inlet to establish the riser flow. The horizontal gas–solid jet was issued through the inlet at 4.3 m above the distributor after 10 s simulation of the riser flow. Real-time simulation of 26 s was completed for each case. Numerical data on

Table 2. Material Properties and Operating Conditions

Property	Value
Particle diameter (μm)	750
Solid density (kg/m^3)	863
Interparticle restitution coefficient	0.8
Particle wall restitution coefficient	0.7
Packed bed voidage	0.346
Angle of internal friction (°)	30
Superficial gas velocity (m/s)	7.62
Solids circulation rate (kg/s)	11.34
Gas viscosity (Pa s)	1.8E−5
Jet inlet diameter (cm)	1.59
Temperature (K)	298
Pressure at top exit (Pa)	101,325
Pressure at bottom (Pa)	111,800
Gas molecular weight (kg/kmol)	28.8

Table 3. Summary of Jet Flow Conditions

Case Name	Voidage at Jet Inlet	Gas Velocity at Jet Inlet (m/s)	Solid Velocity at Jet Inlet (m/s)
Low	0.97	16.64	6.93
High	0.97	37.18	15.5

the flow field variables including pressure, voidage, velocities, and species mass fractions were stored at a frequency of 20 Hz for postprocessing.

Results and Discussion

Riser flow hydrodynamics

To analyze the numerical results, it is important to make sure that the flow has reached the fully developed state. An appropriate criterion is required to justify the flow development. For this purpose, the pressure drop throughout the riser which roughly corresponds to the solids inventory was monitored as shown in Figure 3. At the initial stage, the pressure drop keeps increasing as the solids inventory builds up. It then levels off indicating that the solids circulating pattern has been fully developed and a statistical steady state has been achieved. Similar observation can be obtained through the monitored solids flux at the exit. To avoid the startup effect of such a large system, the first 20 s simulation was excluded from postprocessing and the numerical results were averaged over the remaining 6 s of the simulations when the time-averaged flow field is presented.

The general riser flow hydrodynamics are analyzed by examining the mean flow field. Figures 4 and 5 show the time-averaged voidage and axial solid velocity profiles in a lengthwise cross section aligned with the jet injection as well as several axial cross sections at different elevations. To show the whole picture of lengthwise cross-sectional distribution, the actual height-to-diameter ratio is not preserved and the riser height is scaled down by a factor of 5 in these figures. The typical core-annular flow: a dilute, rapidly rising core flow surrounded by a dense, slowly falling flow adjacent to the wall, can be observed in the riser. Clustering phenomenon is predicted with clusters continuously developing and breaking up, and falling down close to the wall, leading to the core-annular flow pattern.

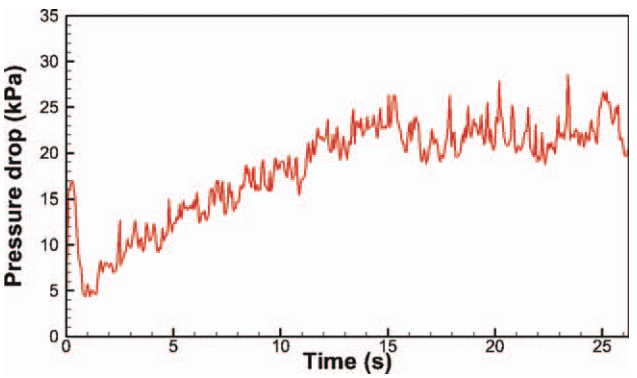

Figure 3. Time variation of the overall pressure drop through the riser for the case with low-jet velocity.

[Color figure can be viewed in the online issue, which is available at wileyonlinelibrary.com.]

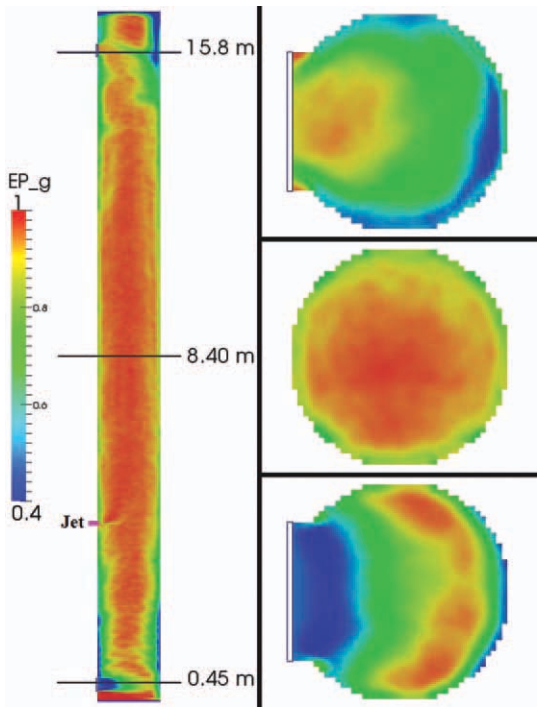

Figure 4. Time-averaged voidage contour in the riser flow for the case with high-jet velocity (the height is scaled down by a factor of 5).

[Color figure can be viewed in the online issue, which is available at wileyonlinelibrary.com.]

Particles close to a loosely packing state are slowly fed into the system through the whole cross section of the solids side-inlet 0.27 m above the bottom distributor. The solid particles through the side-inlet penetrate only a small distance into the riser cross section before they are entrained by the strong upward gas flow through the bottom distributor. The entrained particles are accelerated by the high-velocity gas flow, resulting in increasing voidage along the riser height. Bypassing of gas flow via the other side opposite to the solids inlet is predicted, causing off-center maxima of solid velocity profile downstream. As can be seen in the Figures 4 and 5, the inlet effects are quickly dissipated for this pilot-scale riser and the core-annular structure forms in a short distance above the solids inlet. Similar inlet effects in an pilot-scale riser were reported by De Wilde et al.[37]

In the upper section of the riser, the increase of solids holdup along the height is attributed to the reflection of solid particles from the abrupt exit.[38] The T-shape abrupt exit has a significant influence on the particle velocity. Certain amount of particles escapes through the exit at high velocity. While the rest can not take the sharp turn, they recirculate from the blind T above the outlet port and travel downward along the opposite wall.[39] This can be clearly seen from the solid velocity profile in Figure 5. A region of high particle concentration is formed by the reflected particles at the

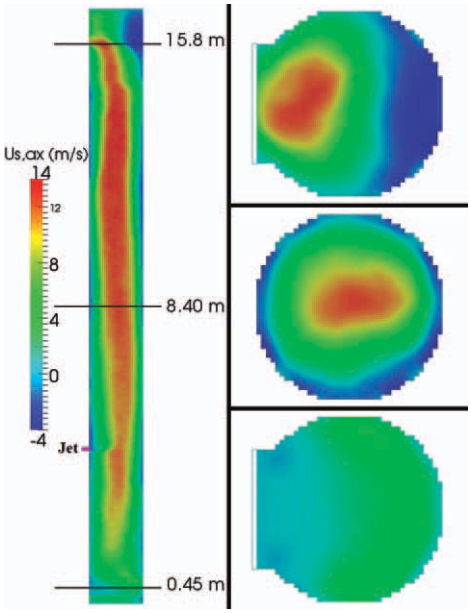

Figure 5. Time-averaged axial solid velocity in the riser flow for the case with high-jet velocity (the height is scaled down by a factor of 5).

[Color figure can be viewed in the online issue, which is available at wileyonlinelibrary.com.]

opposite side of the outlet as depicted in Figure 4. The falling particles cause substantial backmixing below the exit level. As a result, the dilute core of the riser is not located centrally, but shifted toward the exit. The extent of the exit effects propagates down the riser for a few meters, which depends on the operating conditions and the exit restriction such as exit cross-section area.[40,41] Overall, the general flow hydrodynamics of the experimental setup are captured by the current numerical simulations and the influences of both the asymmetric solids inlet and the abrupt exit are reasonably predicted.

Comparison with experimental data

To validate the CFD simulations, quantitative comparisons with the experimental measurements on pressure and solid velocity are made. The overall pressure drop through the riser was predicted to be 21 kPa, which is 23–27% higher than the experimental measurements of 16.5–17 kPa. The overprediction of pressure drop might attribute to the no-slip boundary condition used for the solid phase and the stair-step representation of the cylindrical wall which leads to a larger wall area. In the literature, free-slip,[42] partial-slip,[43] and no-slip wall boundary[44,45] conditions for the solid phase were all used in numerical simulations of circulating fluidized beds. It was reported that a free-slip boundary condition or a partial-slip boundary condition with low friction tends to yield better agreement with the experimental data.[43,46] This conclusion was obtained through two-dimensional or axi-symmetric simulations of riser flows but has not been verified in 3-D simulations. On the other hand, it is generally believed that the wall effect is significant for small lab-scale systems and moderate for pilot-scale columns and probably negligible for large industrial-scale plants.[47] Consequently, the impact of wall boundary condition for the solid phase on the flow hydrodynamics in fully 3-D numerical simulations of such a pilot-scale riser needs further investigation. Another possible reason is that the Superbee scheme employed in the current simulations tends to slightly overpredict the solid inventory compared with other numerical schemes.[48]

In the literature, the axial profile of apparent voidage (or apparent cross-sectional-average solids holdup) is usually reported, which is calculated based on the pressure drop through

$$\Delta P/\Delta L = (1 - \bar{\varepsilon}_g)(\rho_p - \rho_g)g \tag{32}$$

Because of the local acceleration of solid particles and the frictional effect of side wall, the calculated apparent voidage/solids holdup somehow differs from the true value in the system, especially for the lower section of riser.[48–50] This might cause uncertainties in validations when comparing the numerical predictions on axial voidage profile with the experimental data of apparent voidage. Consequently, it is preferential to compare the numerical prediction of pressure gradient with the raw experimental data for the purpose of quantitative validation. Figure 6 presents the comparison between the numerical results and the experimental data on pressure gradient for the case with low-jet velocity. Reasonable agreement between simulation and experiment is obtained though the pressure gradient is slightly overpredicted by the current simulation. Both axial pressure gradient profiles indicate that the apparent solids holdup first decreases with increasing height at the lower region (0–5 m) and remains fairly constant in the middle region (5–10 m) and then, increases with height at the upper region of the riser (10–15 m). It is consistent with the lengthwise cross-sectional voidage profile in Figure 4 and this "C"-shaped pressure curve is representative for the NETL CFB plant.

Figures 7 and 8 compare the radial profiles of axial solid velocity to the experimental data measured by a fiber optic probe at 0.15 m above the feed injection in the same azimuthal plane for the riser flow with low- and high-jet velocities, respectively. For the riser flow with low-jet velocity, experimental data of nine repeated runs were analyzed and the error bars representing the standard deviation are shown in the figure. While for the case with high-jet velocity, only two experimental data sets measured in a single run are shown. Overall, reasonable agreement between the numerical simulations and the experimental measurements is obtained. For both cases, high-solid velocity in the central core and negative solid axial velocity close to the wall are predicted. The high-velocity core shifts toward the opposite side of the jet inlet, which is probably caused by the solids inlet and outlet, as well as the injection of gas–solid jet. However, a further investigation is needed to distinguish the effect of jet injection from that of solids inlet and outlet.

Influence of jet injection

The influence of horizontal gas–solid jet on the riser flow hydrodynamics is analyzed though the time-averaged voidage and solid velocity distributions. Figures 9 and 10 show voidage and axial solid velocity distributions in the region where the jet is introduced. The axial cross-sectional views

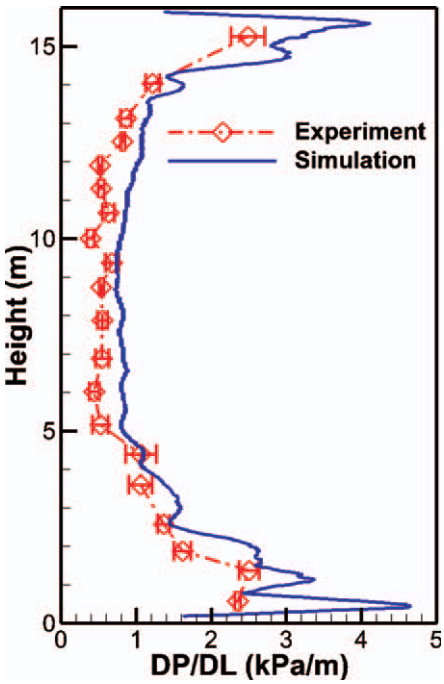

Figure 6. Axial profiles of pressure gradient for the case with low-jet velocity (experiment data on pressure gradient were obtained by averaging data measured in 12 duplicated runs with error bar representing the standard deviation).

[Color figure can be viewed in the online issue, which is available at wileyonlinelibrary.com.]

at the jet level and 0.10 m above and below the jet inlet are also shown in these figures. These figures demonstrate the influence of jet on the overall flow hydrodynamics in the riser. For both cases, the jet acts as a cylindrical obstacle with a deformable surface from the main flow leading to particles accumulation in front of it. The impact becomes more pronounced for the high-jet velocity though it is still very localized. In addition, the injected particles with a higher

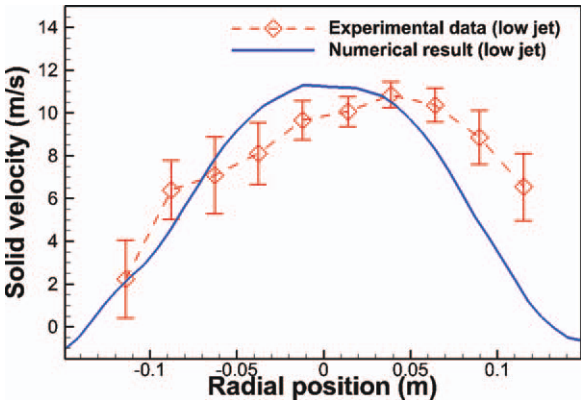

Figure 7. Radial profile of axial solid velocity 15 cm above the jet injection for the case with low-jet velocity (experimental data were obtained by averaging 16 data sets measured in nine runs).

[Color figure can be viewed in the online issue, which is available at wileyonlinelibrary.com.]

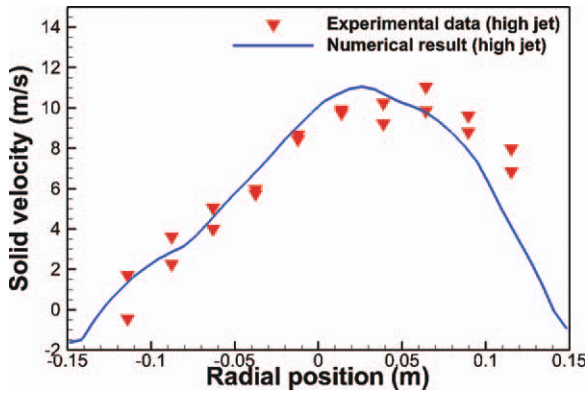

Figure 8. Radial profile of axial solid velocity 15 cm above the jet injection for the case with high-jet velocity (two experimental data sets measured in a single run was shown).

[Color figure can be viewed in the online issue, which is available at wileyonlinelibrary.com.]

radial component of momentum penetrate farther than the gas into the cross-flow, which also contributes to the formation of the dense region in front of the jet. Figure 9 shows that the injected gas flow dilutes the riser flow in the downstream region near the wall which is more visible for the high-jet velocity. The influence of jet injection on the axial solid velocity distribution is more pronounced above the injection level, especially for the high-jet velocity. Away from the wall region, the particles below the jet flowing upward are entrained into the jet and are transported deeper along the jet direction. A close view at the jet inlet in both figures reveals that the jet disrupts the downward flow along the wall and a small region with low solids concentration right below the jet inlet is formed, which is similar to the effect of secondary air jets.[47] In addition, the high-velocity jet tends to promote the downward motion of particles close to the left wall in Figure 10 above the injection level, when compare the axial velocity profiles for low- and high-jet velocities.

Secondary gas injection through radial and tangential jets into circulating fluidized beds has been studied by several researchers. It was reported that the secondary gas injection, usually 30–50% of the total fluidization air, increased the solids holdup in the riser considerably and profoundly affected the hydrodynamics.[51–53] However, this conclusion is not applicable to the current situation. In the above analyses, the flow pattern is affected by the jet injection only in a short distance up and downstream. This is because the flow rate through jet injection is very small compared to the riser flow. Even for the case with high-jet velocity, the gas and solids flow rates through the jet inlet are only 1.3% and 0.7% of that though the riser cross section, respectively. No significant cut-off effect of the secondary air jets blocking the rising gas–solid suspension reported before[51–53] can be observed in the current study. Hence, the influence of horizontal gas–solid injection on the overall flow hydrodynamics is relatively limited.

Jet behavior

As the purpose of gas–solid jets is to feed reactants to the reactor, understanding of the injection and dispersion behavior

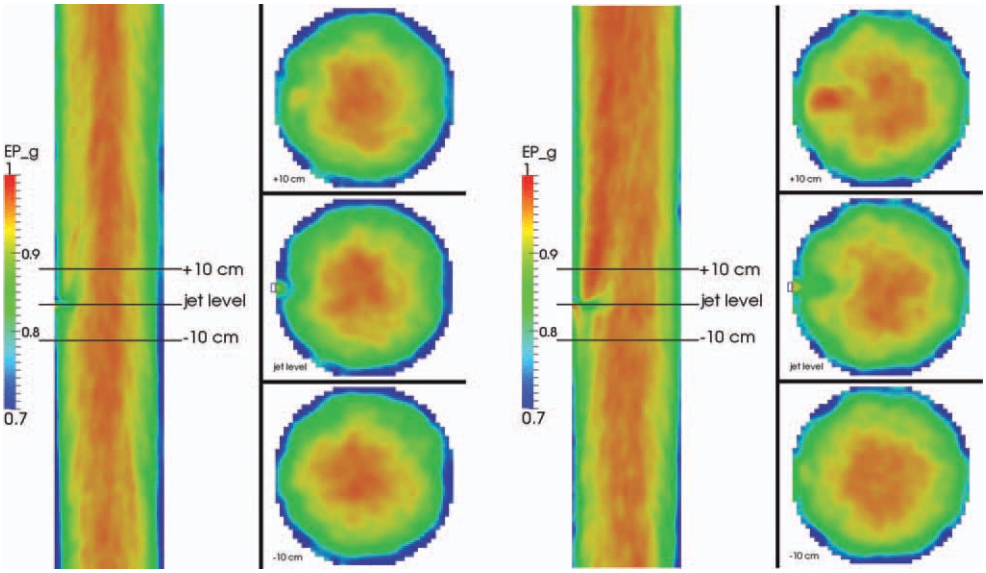

Figure 9. Time-averaged voidage contour in the jet region for low-jet velocity (left) and high-jet velocity (right).

[Color figure can be viewed in the online issue, which is available at wileyonlinelibrary.com.]

of particles under such conditions would allow optimization of the solids injectors. The behavior of gas–solid jet is studied by analyzing the transient tracer distributions inside the riser flow. In the current numerical simulations, gas and particles injected through the jet were treated as tracer species in gas and solid phases, respectively. Transport equations were solved for the mass fraction of each species. To track the jet movement, concentrations of tracer gas and particles are calculated by

$$\varepsilon_{g,tr} = \varepsilon_g X_{g,tr} \tag{33}$$

$$\varepsilon_{p,tr} = \varepsilon_p X_{p,tr} \tag{34}$$

where $X_{g,tr}$ and $X_{p,tr}$ are species mass fractions of tracer gas and particles, respectively.

Figure 11 shows snapshots of voidage, concentrations of tracer particles, and tracer gas. The gas–solid jet is observed to be very unstable and is greatly affected by the gas–solid crossflow, especially by the clusters. Generally, the cross section of the jet deforms from a circle at the inlet to a kidney- or horseshoe-like shape deeper in the far jet region, which is not shown in the figure. The jet is finally broken up by the strong fluctuating crossflow. During this process, large clusters play the dominant role in affecting the shape of jet. Because of the mainly upward crossflow and the buoyancy effect, the jet migrates upward. Occasionally, large falling clusters close to the wall drag the jet and bend it downward. As the jet propagates into the crossflow, the continuous dense region formed in front of the jet breaks up and the tracer particles aggregate into clusters as shown in the upper

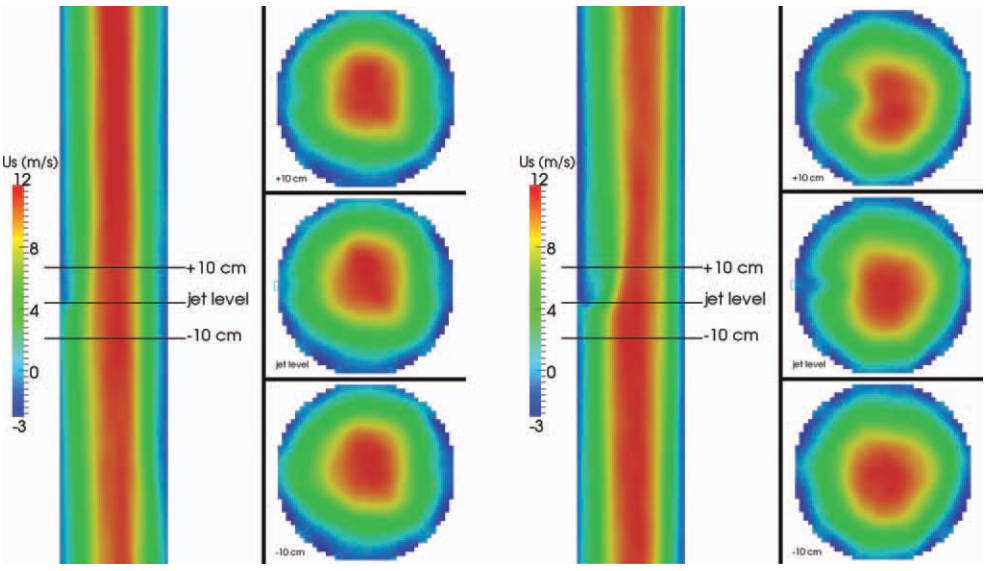

Figure 10. Time-averaged axial solid velocity in the jet region for low-jet velocity (left) and high-jet velocity (right).

[Color figure can be viewed in the online issue, which is available at wileyonlinelibrary.com.]

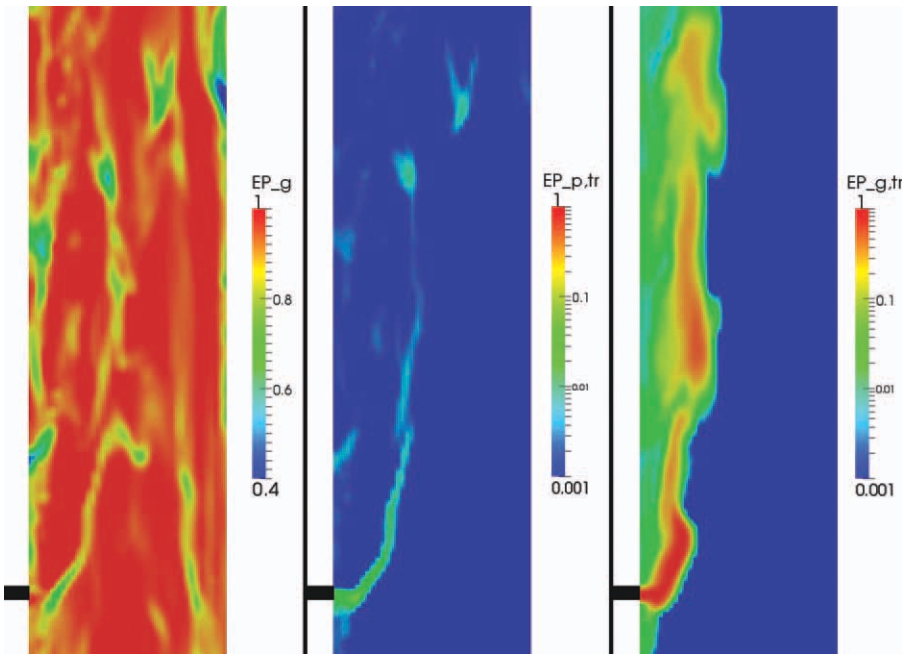

Figure 11. Snapshots of voidage, concentrations of tracer particles, and gas for high-jet velocity (From left to right: voidage, tracer particle concentration, tracer gas concentration).

[Color figure can be viewed in the online issue, which is available at wileyonlinelibrary.com.]

region of the tracer particle concentration plot in Figure 11. Both tracer gas and tracer particles distributions are not uniform because of the nonhomogeneous crossflow. The tracer particles with high momentum travel deeper into the crossflow and separate from the jetting gas flow because of different dynamic responses of gas and particles to the crossflow. The effect of separation is twofold. On one hand, the solids penetrate deeper into the crossflow resulting in enhanced solids mixing, which is confirmed in the mixing study below. In addition, for heterogeneous reactions controlled by heat transfer, the separation of gas and particles after entering the crossflow eliminates the cooling effect on reactions caused by the jetting gas. On the other hand, in some processes, for example, some coal gasifier designs, the air–coal mixture is expected to undergo combustion reactions to supplement heat needed by the endothermic gasification reactions. Under such circumstance, separation of the coal particles from the air jet not only limits the desired combustion but also leads to a cool region of oxygen-rich gas. The cool oxygen-rich gas flow propagates upward and might cause unwanted combustion of the devolitization and gasification product gases.[54] Hence, the separation of gas and solids should be taken into account in design for the desired performance when they are injected together into the reactor crossflow. From the experimental point of view, the gas–solid separation suggests that both jetting gas and particles need to be tracked to study the gas–solid jet behavior. In Figure 11, the nonzero tracer concentration below the jet injection level indicates backmixing of gas and solids, which will be discussed later.

Jet penetration

Among many parameters describing the jet issuing into a gas–solid crossflow, jet penetration depth is one of the most important since it determines the length of the effective interaction zone between the jetting material and the crossflow. There are many empirical correlations for predicting the gas/liquid jet penetration in dense fluidized beds.[1–3] However, no such correlation is available for the gas–solid jet. Even a clear definition of jet penetration is not straightforward as the jet boundary is hard to define for the two-phase jet with strong-phase separation.[22]

In the experiments conducted at NETL, jet penetration was characterized by the radial distance of the peak tracer concentration and the half-height width of the peak profile at different downstream elevations, as schematically shown in Figure 2. Similar approach is adopted in the numerical simulations to estimate the jet penetration. Lateral profiles of tracer particles concentration at 0.15 and 0.30 m above the jet inlet are presented in Figure 12 for the case with high-jet velocity. The location of peak and the half-height width are determined and compared with the experimental measurements in Tables 4 and 5 at these two elevations. Both the peak distance and the half-height width increase with jet velocity. The latter is caused by the stronger fluctuations of the gas–solid jet with higher velocity. Generally, predictions of the peak locations compare favorably to the experimental data. However, the half-height widths are substantially underpredicted by the numerical simulations. The underprediction is attributed to the unstable gas–solid flow through the feed nozzle for which the solids concentration, gas, and solids velocities subject to strong fluctuations at the jet inlet in the experiments. This was not considered in the current simulations where a constant flow condition was specified at the jet inlet. In addition, the simplification of the gas-phase turbulence modeling may be another reason to the underprediction of half-height width as the complex effect of gas turbulence on the solid dispersion, which was not included in the current study, might be

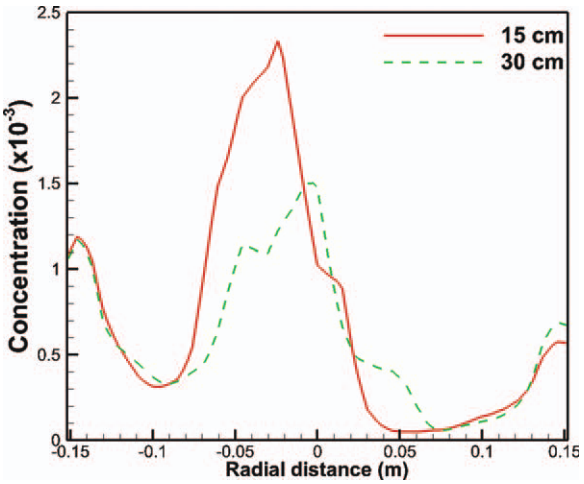

Figure 12. Profiles of tracer particles concentration at different levels above the jet port for high-jet velocity.

[Color figure can be viewed in the online issue, which is available at wileyonlinelibrary.com.]

important though the dispersion of tracer particles is believed to be dominated by the flow convection.

Similar analyses were performed based on the tracer gas concentration profiles. Penetration of the jetting gas is smaller than the jetting particles because of its lower momentum. The gas jet characteristics are not reported here as no such measurements are available in the experiments for comparison. Research in this area at NETL is ongoing and more discussions on the gas–solid jet penetration analyses will be reported elsewhere.[55]

Feed mixing

Gas mixing in fluidized beds is critical to conversions and selectivities of various industrial processes. Likewise, the solids mixing in CFB risers affects the gas–solid contacting, suspension-to-wall heat transfer, the degree of catalyst deactivation, and particle conversion for gas–solid reactions.[56] Hence, it is of practical importance to study the mixing of feed through the horizontal jet with the bulk materials inside the reactor.

Time-averaged mass fractions of tracer gas and particles close to the jet injection are shown in Figures 13 and 14 to study mixing of the gas–solid injection with the bed materials. Clearly, the radial mixing is much slower than the axial mixing or dispersion along the riser height, leading to large gradients of concentration in the radial direction. According to previous studies, secondary air injection enhances the lateral/radial gas mixing in circulating fluidized beds.[53,57] Consequently, better mixing of the jetting gas and solids with the crossflow is expected for the case with high-jet velocity. Jet penetration depth is a key parameter affecting the mixing behavior. As can be seen in both figures, the deeper penetration of gas and solids for the high-velocity jet leads to a better radial mixing in the downstream region, especially for the solids mixing. Similarly, the smaller penetration of gas than particles accounts for the poorer radial gas mixing than the radial solids mixing for the same case. The results discussed here might suggest that multiple jets should be used to achieve a better feed mixing with the riser crossflow.

Table 4. Predictions of Jet Characteristics at 0.15 m Above the Injection

Case	Num. Peak Location (m)	Num. Half-Height Width (m)	Exp. Peak Location (m)	Exp. Half-Height Width (m)
Low-jet velocity	0.062	0.052	0.08	0.13
High-jet velocity	0.128	0.064	0.13	0.18

Table 5. Predictions of Jet Characteristics at 0.30 m Above the Injection

Case	Num. Peak Location (m)	Num. Half-Height Width (m)	Exp. Peak Location (m)	Exp. Half-Height Width (m)
Low-jet velocity	0.064	0.048	0.08	0.15
High-jet velocity	0.15	0.072	0.14	0.17

The overall mixing behavior in the riser with low- and high-jet velocities are shown in Figure 15 in which distributions of mass fractions of tracer gas and particles are shown in the lengthwise cross-sectional planes aligned with and normal to the horizontal jet. For ease of presentation, the height is again scaled down by a factor of 5. The effect of T-shape abrupt exit on mixing is illustrated in these figures. Significant solids backflow caused by the abrupt exit affects the mixing of solids injection with the riser flow to certain extent.[40] The strong backflow brings the tracer at the exit level back to the riser, resulting in high concentration close to the wall opposite the exit. Although the exit effect is almost identical for cases with low- and high-jet velocity, different mixing behaviors at the exit level are observed because of different extents of radial mixing and feeding flow rates. Furthermore, limited radial mixing has a profound influence on the downstream mixing of tracer gas and bulk flow. For the case with low-jet velocity, the gas jet barely reaches center of riser leading to low tracer concentration in the center of the riser along the entire height. Although, for the case with high-jet velocity, the tracer concentration becomes more uniform than that of low-jet velocity, especially for the tracer particles distribution. In Figure 15, high concentrations close to the wall are attributed to the backmixing caused by the downward solids flow. For fast reactions such as FCC process, the solids backmixing is undesirable. Whereas, for some processes such as CFB coal combustion increasing the resident time of the coal due to backmxing gives more efficient combustion and greater suspension density at the riser top and enhances heat transfer in that region.[40]

By comparing the concentration distributions below the jet level in Figure 15, it seems that the backmixing of the gas–solid feed increases with the jet velocity. However, it should be noted that tracer flow rates are different for these two cases. An accurate way is needed to evaluate the influence of jet velocity on the feed mixing with the bed materials. For this purpose, the specific concentrations of tracer gas, C_g/C_{g0}, and particles, C_s/C_{s0}, are compared. C_g and C_s are volume fractions of tracer gas and particles in gas and solids phases, respectively. The exit tracer concentration, C_{g0}, is defined as

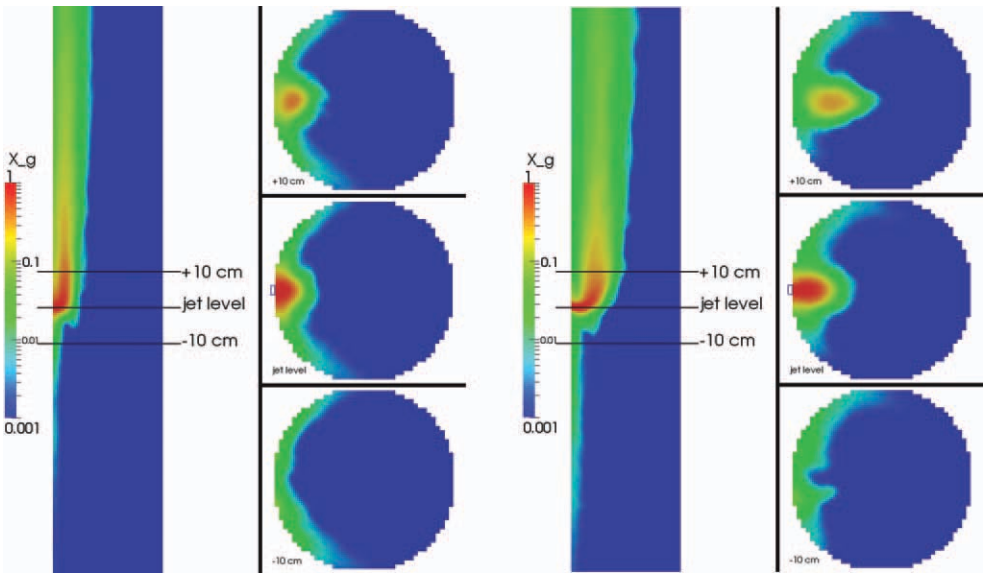

Figure 13. Time-averaged mass fraction of tracer gas for low-jet velocity (left) high-jet velocity (right).

[Color figure can be viewed in the online issue, which is available at wileyonlinelibrary.com.]

$$C_{g0} = Q_{g,tracer}/Q_g \tag{35}$$

where $Q_{g,tracer}$ is the volumetric flow rate of tracer at the injector and Q_g is the total gas flow rate at the exit. Similarly, the exit concentration of tracer particle is calculated as

$$C_{s0} = Q_{s,tracer}/Q_s \tag{36}$$

where $Q_{s,tracer}$ is the volumetric flow rate of tracer particles at the injector and Q_s is the total solids circulation rate. Figures 16 and 17 show the distributions of specific concentration of tracer gas and particles at different levels below the jet injection. As can be seen from the comparison, the backmixing tends to decrease as the jet velocity increases, which is consistent with previous studies on horizontal gas jets in a bubbling fluidized bed.[5]

It should be noted that gas and solids mixing in the above discussions refer to the mixing of feed through jet injection with the riser crossflow. This differs from the mixing obtained from most experimental studies in which the tracer is usually injected as a point source at the center of riser or uniformly below the distributor. In addition, it is expected that the overall mixing inside the riser flow is not greatly affected by the gas–solid injection considering its local impact on the flow hydrodynamics as already discussed before. To confirm this, a dedicated experiment on gas and solids mixing is needed.

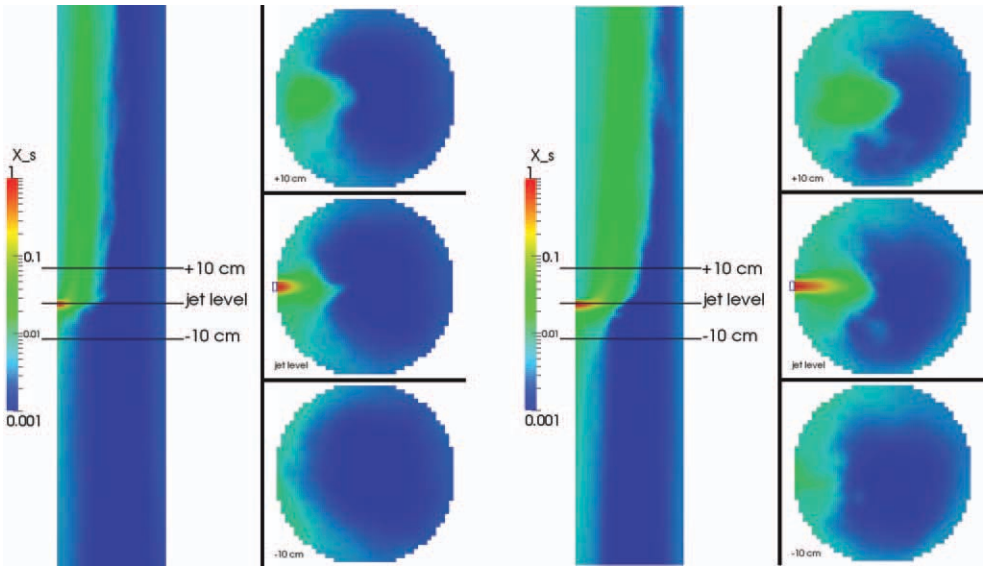

Figure 14. Time-averaged mass fraction of tracer particles for low-jet velocity (left) (b) high-jet velocity. (right)

[Color figure can be viewed in the online issue, which is available at wileyonlinelibrary.com.]

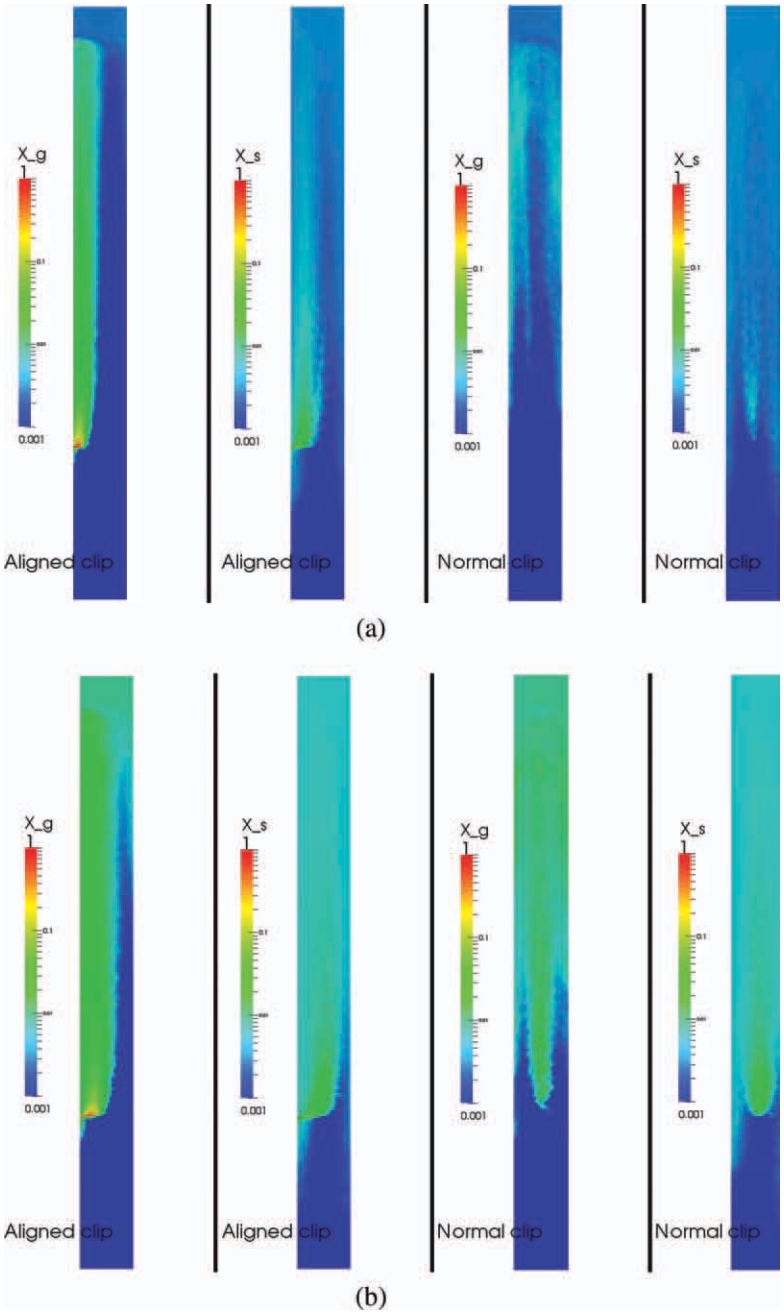

Figure 15. Distributions of time-averaged mass fraction of tracer gas and particles for (a) low-jet velocity; (b) high-jet velocity (the height is scaled down by a factor of 5).

[Color figure can be viewed in the online issue, which is available at wileyonlinelibrary.com.]

Summary and Conclusions

In this study, a horizontal gas–solid jet in a high-density riser flow was investigated with high-resolution CFD simulations. A comprehensive investigation was carried out to study the hydrodynamics aspects of gas–solid injection in a circulating fluidized bed as well as mixing of feed with bulk materials. The impacts of the gas–solid injection on the riser flow hydrodynamics were evaluated with respect to voidage and solids velocities distributions. The influence of the studied horizontal gas–solid injections on the overall flow hydrodynamics was found to be relatively localized and mainly in the downstream region. However, the jet was very unstable and its behavior was greatly affected by the nonhomogeneous riser flow, especially by the clusters. Substantial separation of jetting gas and solids after they enter the riser flow was predicted in the numerical simulations, which needs to be considered in process design and optimization. The jet penetrations at different downstream levels were studied and reasonable agreement with the experimental measurements at NETL was obtained. The mixing behavior of the gas and particles injected through the jet flow with the bed materials was analyzed. The radial mixing at the injection level had a profound influence on the downstream mixing between jetting material and bulk flow and the jet

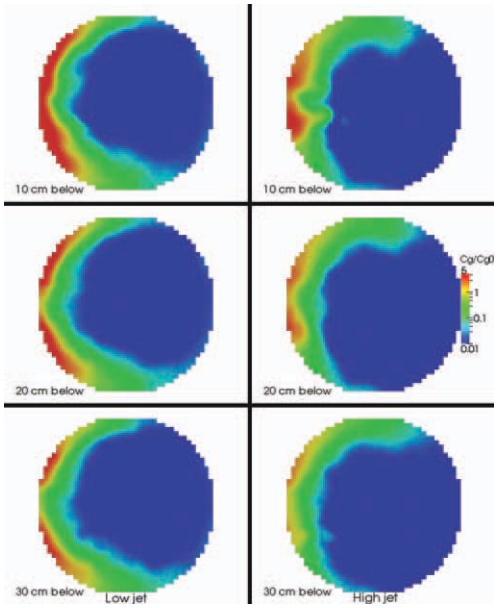

Figure 16. Specific concentrations of tracer gas at different levels below the jet injection.

[Color figure can be viewed in the online issue, which is available at wileyonlinelibrary.com.]

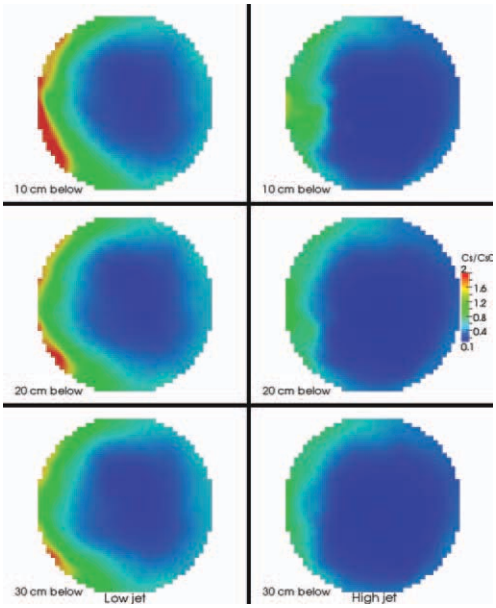

Figure 17. Specific concentrations of tracer particles at different levels below the jet injection.

[Color figure can be viewed in the online issue, which is available at wileyonlinelibrary.com.]

penetration was found to be the key parameter affecting radial mixing. Backmixing of the jetting gas and solids was also evaluated, which decreases as the jet velocity increases. The current CFD simulations were demonstrated to be a very useful tool to study the gas–solid jet in high-density riser flows.

Acknowledgments

The authors thank Drs. Lawrence Shadle, Christopher Ludlow, and James Spenik for providing detailed experimental data and useful discussions. This technical effort was performed in support of the National Energy Technology Laboratory's ongoing research in advanced multiphase flow simulation under the RES contract DE-FE0004000. This research was also supported in part by an appointment to the National Energy Technology Laboratory Research Participation Program, sponsored by the U.S. Department of Energy and administrated by the Oak Ridge Institute for Science and Education.

Notation

Symbols

C = concentration
d_p = particle diameter, m
D_{g0} = molecular diffusivity, m^2/s
e = coefficient of restitution for particle collision
e_w = particle wall restitution coefficient
g = gravitational acceleration, m/s^2
g_0 = radial distribution function
l = turbulence length scale, m
P = gas pressure, Pa
P_s = solid frictional pressure, Pa
Q = volumetric flow rate, m^3/s
$\vec{V}$ = velocity, m/s
x, y, z = Cartesian coordinates with z vertical and x lateral, m
X = species mass fraction

Greek letters

ε_g = volume fraction of gas
ε_p = volume fraction of particles
$\varepsilon_{p,max}$ = maximum volume fraction of particles
μ_p = solid viscosity, Pa s
Θ_p = granular temperature, J/kg
ρ_g = gas density, kg/m^3
ρ_p = solid density, kg/m^3

Subscript

g = gas phase
p,s = solid phase
tr,tracer = tracer

Literature Cited

1. Hong R, Li H, Li H, Wang Y. Studies on the inclined jet penetration length in a gas-solid fluidized bed. *Powder Technol*. 1997;92:205–212.
2. Merry JMD. Penetration of a horizontal gas jet into a fluidised bed. *Trans Inst Chem Eng Chem Eng*. 1971;49:189–195.
3. Ariyapadi S, Berruti F, Briens C, McMillan J, Zhou D. Horizontal penetration of gas-liquid spray jets in gas-solid fluidized beds. *Int J Chem React Eng*. 2004;2:A22.
4. Li T, Pougatch K, Salcudean M, Grecov D. Numerical simulation of single and multiple gas jets in bubbling fluidized beds. *Chem Eng Sci*. 2009;64:4884–4898.
5. Li T, Pougatch K, Salcudean M, Grecov D. Mixing of secondary gas injection in a bubbling fluidized bed. *Chem Eng Res Des*. 2009;87:1451–1465.
6. Bruhns S, Werther J. An investigation of the mechanism of liquid injection into fluidized beds. *AIChE J*. 2005;51:766–775.
7. Skouby DC. Hydrodynamic studies in a 0.45-m riser with liquid feed injection. *AIChE Symp Ser*. 1999;321:67–70.
8. Zhu C, Wang XH, Fan LS. Effect of solids concentration on evaporative liquid jets in gas-solid flows. *Powder Technol*. 2000; 111:79–82.
9. Li T, Pougatch K, Salcudean M, Grecov D. Numerical simulation of an evaporative spray in a gas-solid crossflow. *Int J Chem React Eng*. 2010;8:A43.
10. Glicksman L, Carr E, Noymer P. Particle injection and mixing experiments in a one-quarter scale model bubbling fluidized bed. *Powder Technol*. 2008;180:284–288.
11. Shadle L, Ludlow JC, Spenik J, Seachman S, Guenther C. *Jet penetration into a riser operated in dense suspension upflow: experimental and model comparisons*. In: *Circulating Fluidized Bed IX*. eds. Werther J Hamburg, Germany: Tutech Innovation, 2008; 307-312.

12. Wang F, Yu Z, Marashdeh Q, Fan LS. Horizontal gas and gas/solid jet penetration in a gas-solid fluidized bed. *Chem Eng Sci*. 2010;65:3394–3408.
13. Syamlal M, Guenther C, Cugini A, Ge W, Wang W, Yang N, Li J. Computational science: Enabling technology development. *Chem Eng Prog*. 2011; 107:23-29.
14. Grace JR, Li T. Complementarity of CFD, experimentation and reactor models for solving challenging fluidization problems. *Particuology* 2010;8:498–500.
15. Watanabe H, Otaka M. Numerical simulation of coal gasification in entrained flow coal gasifier. *Fuel* 2006;85:1935–1943.
16. Fletcher DF, Haynes BS, Christo FC, Joseph SD. A CFD based combustion model of an entrained flow biomass gasifier. *Appl Math Model*. 2000;24:165–182.
17. Vicente W, Ochoa S, Aguillon J, Barrios E. An Eulerian model for the simulation of an entrained flow coal gasifier. *Appl Therm Eng*. 2003;23:1993–2008.
18. Chen CX, Horio M, Kojima T. Numerical simulation of entrained flow coal gasifiers. Part I: modeling of coal gasification in an entrained flow gasifier. *Chem Eng Sci*. 2000;55:3861–3874.
19. Chen CX, Horio M, Kojima T. Numerical simulation of entrained flow coal gasifiers. Part II: effects of operating conditions on gasifier performance. *Chem Eng Sci*. 2000;55:3875–3883.
20. Silaen A, Wang T. Effect of turbulence and devolatilization models on coal gasification simulation in an entrained-flow gasifier. *Int J Heat Mass Transf*. 2010;53:2074–2091.
21. Chen CX, Horio M, Kojima T. Use of numerical modeling in the design and scale-up of entrained flow coal gasifiers. *Fuel* 2001;80:1513–1523.
22. Li T, Gel A, Syamlal M, Guenther C, Pannala S. High resolution simulations of coal jets in a gasifier. *Ind Eng Chem Res*. 2010; 49:10767–10779.
23. Mei JS, Monazam ER, Shadle LJ. Flow regime study of a light material in an industrial scale cold flow circulating fluidized bed. *J Energy Resour Technol Trans ASME*. 2006;128:129–134.
24. Benyahia S, Syamlal M, O'Brien TJ. Summary of MFIX. Equations 2005–4. From URL https://mfix.netl.doe.gov/documentation/MFIX-Equations2005-4-4.pdf, August 2008.
25. Syamlal M, Rogers W, Brien TJO. *MFIX Documentation: Theory Guide*. Morgantown, West Virginia: U.S. Department of Energy (DOE), Morgantown Energy Technology Center, 1993.
26. Gidaspow D. *Multiphase flow and fluidization: continuum and kinetic theory descriptions*. Boston: Academic Press, 1994.
27. Lun CKK, Savage SB, Jeffrey DJ, Chepurniy N. Kinetic theories for granular flow - inelastic particles in Couette-flow and slightly inelastic particles in a general flowfield. *J Fluid Mech*. 1984;140: 223–256.
28. Sinclair JL, Jackson R. Gas-particle flow in a vertical pipe with particle-particle interactions. *AIChE J*. 1989;35:1473–1486.
29. Deardorf JW. Magnitude of subgrid scale eddy coefficient. *J Comput Phys*. 1971;7:120–133.
30. Crowe CT, Troutt TR, Chung JN. Numerical models for two-phase turbulent flows. *Annu Rev Fluid Mech*. 1996;28:11–43.
31. Enwald H, Peirano E, Almstedt AE. Eulerian two-phase flow theory applied to fluidization. *Int J Multiphase Flow*. 1996;22:21–66.
32. Portela LM, Oliemans RVA. Possibilities and limitations of computer simulations of industrial turbulent dispersed multiphase flows. *Flow Turbulence Combust*. 2006;77:381–403.
33. Hsiau SS, Hunt ML. Kinetic-theory analysis of flow-induced particle diffusion and thermal conduction in granular material flows. *J Heat Transf Trans ASME*. 1993;115:541–548.
34. Andrews AT, Loezos PN, Sundaresan S. Coarse-grid simulation of gas-particle flows in vertical risers. *Ind Eng Chem Res*. 2005; 44:6022–6037.
35. Guenther C, Syamlal M, Longanbach J, Smith P. CFD modeling of a transport gasifier, Part II. In: *Proceedings of the 20th Annual Pittsburgh Coal Conference*, Pittsburgh, PA, 2003.
36. Guenther C, Syamlal M. The effect of numerical diffusion on simulation of isolated bubbles in a gas-solid fluidized bed. *Powder Technol*. 2001;116:142–154.
37. De Wilde J, Van Engelandt G, Heyndenickx GJ, Marin GB. Gas-solids mixing in the inlet zone of a dilute circulating fluidized bed. *Powder Technol*. 2005;151:96–116.
38. Mei JS, Shadle LJ, Yue PC, Monazam ER. Flow regime study in a high density circulating fluidzied bed riser with an abrupt exit. In: 12th International Conference on Fluidization - New Horizons in Fluidization Engineering. Eds. Berruti F, Bi X, Pugsley T. *Engineering Conferences International*, 2007; 63–70.
39. Mei J, Lee G, Seachman S, Ludlow JC, Shadle L. *Flow regime study in a circulating fluidized bed riser with an abrupt exit: high density suspension*. In: *Circulating Fluidized Bed IX*. eds. Werther J Hamburg, Germany: Tutech Innovation, 2008; 177–182.
40. Cheng Y, Wei F, Yang GQ, Jin Y. Inlet and outlet effects on flow patterns in gas-solid risers. *Powder Technol*. 1998;98:151–156.
41. De Wilde J, Marin GB, Heynderickx GJ. The effects of abrupt T-outlets in a riser: 3D simulation using the kinetic theory of granular flow. *Chem Eng Sci*. 2003;58:877–885.
42. Zhang DZ, VanderHeyden WB. High-resolution three-dimensional numerical simulation of a circulating fluidized bed. *Powder Technol*. 2001;116:133–141.
43. Almuttahar A, Taghipour F. Computational fluid dynamics of high density circulating fluidized bed riser: Study of modeling parameters. *Powder Technol*. 2008;185:11–23.
44. Hansen KG, Ibsen CH, Solberg T, Hjertager BH. Eulerian/Eulerian CFD simulation of a cold flowing FCC riser. *Int J Chem React Eng*. 2003;1:A31.
45. Ibsen CH, Solberg T, Hjertager BH. Evaluation of a three-dimensional numerical model of a scaled circulating fluidized bed. *Ind Eng Chem Res*. 2001;40:5081–5086.
46. Benyahia S, Syamlal M, O'Brien TJ. Evaluation of boundary conditions used to model dilute, turbulent gas/solids flows in a pipe. *Powder Technol*. 2005;156:62–72.
47. Grace JR, Bi X, Golriz M. *Circulating fluidized beds*. In: Yang W-C, editor, *Handbook of Fluidization and Fluid-Particle Systems*. New York: Marcel Dekker, 2003.
48. Guenther C, Syamlal M, Shadle L, Ludlow C. A numerical investigation of an industrial scale gas-solids CFB. In: *Proceedings of the 7th International Conference on Circulating Fluidized Beds*, Niagra Falls, Ontario, Canada, 2002.
49. Arena U, Cammarota A, Pistone L, Tecchio PV. *The high velocity fluidization behavior of solids in a laboratory scale circulating bed*. In: *Circulating Fluidized Bed Technology*. New York: Pergamon Press, 1986.
50. Issangya AS, Bai D, Bi HT, Lim KS, Zhu J, Grace JR. Suspension densities in a high-density circulating fluidized bed riser. *Chem Eng Sci*. 1999;54:5451–5460.
51. Cho YJ, Namkung W, Kim SD, Park SW. Effect of secondary air injection on axial solid holdup distribution in a circulating fluidized-bed. *J Chem Eng Jpn*. 1994;27:158–164.
52. Kang Y, Song PS, Yun JS, Jeong YY, Kim SD. Effects of secondary air injection on gas-solid flow behavior in circulating fluidized beds. *Chem Eng Commun*. 2000;177:31–47.
53. Koksal M, Hamdullahpur F. Gas mixing in circulating fluidized beds with secondary air injection. *Chem Eng Res Des*. 2004;82:979–992.
54. Syamlal M, Guenther C, Gel A, Pannala S. High performance computing: clean coal gasifier designs using hybrid parallelization. *Presented at the Fluidization XIII*, Gyeong-ju, Korea, 2010.
55. Li T, Guenther C. High-resolution simulations of gas-solids jet penetration into a high density riser flow. In: *Proceedings of the International Conference on Circulating Fluidized Beds and FluidiZed Bed Technology*. Eds. Knowlton T, New York: Engineering Conference International, In press.
56. Bi X. Gas and solid mixing in high-density CFB risers. *Int J Chem React Eng*. 2004;2:A12.
57. Namkung W, Kim SD. Radial gas mixing in a circulating fluidized bed. *Powder Technol*. 2000;113:23–29.

Manuscript received Dec. 9, 2010, and revision received Mar. 1, 2011.